Control of Shunt Active Power Filter based on Z-Source Inverter Fed by PV System

Ahfouda Abdelkarim
Department of Electrical engineering, LEVRES Labs, University of El-Oued, El-Oued, Algeria
KarimdzKarim03@gmail.com

Bekakra Youcef
Department of Electrical engineering, LEVRES Labs, University of El-Oued, El-Oued, Algeria
youcef1984@gmail.com

Djaafar Toumi
VTRS-Research Laboratory, University of El-Qued, El-Qued, Algeria
toumi-djaafar@univ-eloued.dz

Laid Zellouma
Department of Electrical engineering, LEVRES Labs, University of El-Oued, El-Oued, Algeria
Zellouma13@yahoo.fr

Hettiri Messaoud
Department of Electrical University of El-Oued, El-Oued, Algeria
Hettiri-messaoud@univ-eloued.dz

Ahmed Ibrahim
Faculty of engineering, Zagazig university, Egypt
ibragim@tpu.ru.

***Abstract*—This paper proposes the integration of a Z-Source Inverter (ZSI)-based Shunt Active Power Filter (SAPF) with a Photovoltaic (PV) system to enhance power quality. The ZSI offers significant advantages over traditional inverters, including improved boost functionality, reduced harmonics, and higher performance. The SAPF control in this study utilizes a trigonometric method, with a proportional-integral (PI) controller employed to regulate the DC-link voltage. The primary objective of this paper is to eliminate total harmonic distortion (THD) in the source current. To validate the proposed method, extensive simulations were conducted using MATLAB/Simulink under various operating conditions. The results obtained provide conclusive evidence of the effectiveness of the proposed approach in achieving its objectives**

***Index Terms*—component, Photovoltaic system, Shunt active power filter, trigonometric method, Z-source inverter, total harmonic distortion.**

I. INTRODUCTION

The increasing use of non-linear loads in industrial applications has led to undesirable effects on power quality [1][2]. The prominent issues in power quality include distortions in current, voltage, and frequency, which significantly impact consumers. With the growing reliance on sensitive devices that require clean sine waveforms, the demand for consistent power quality has escalated [3][4]. To address the challenges posed by harmonic currents and power-related problems caused by non-linear loads, numerous studies have been conducted. Passive filters have traditionally been employed to suppress current harmonics and mitigate energy pollution in the network over extended periods. However, these filters have inherent drawbacks such as large size, considerable weight, and susceptibility to dynamic parameters that can lead to resonance issues. Active filters emerged as a solution in the 1970s, effectively overcoming these challenges [5][6]. Shunt Active Power Filters (SAPFs) provide a versatile solution for mitigating harmonic currents and correcting power factors. They possess the capability to adapt to various load types. The SAPF configuration involves a voltage/current source inverter interacting with a link capacitor connected in parallel with non-linear loads [7][8]. The electrical converter generates the necessary harmonic elements to suppress harmonic currents drawn by non-linear loads, thereby ensuring that the main current remains sinusoidal and in phase with the supply voltage [9][10]. Due to the increasing penetration of renewable energy sources, there have been significant advancements in classic shunt active filters, wherein a renewable energy source is connected to the DC side of the filter to reduce energy consumption from the electrical grid. Consequently, filters have gained immense importance [11][12].

The latter possesses numerous advantages, such as harmonic current elimination, reactive power compensation, and simultaneous active power injection. However, it also suffers from several disadvantages, such as non-linear properties and a strong reliance on environmental conditions. Consequently, there is a pressing need for accurate monitoring of the maximum energy obtained from photovoltaic sources[13]. To address this issue, various maximum power point tracking (MPPT) techniques have been proposed in the literature. One such technique is the perturbation and observation (P&O) technique, which involves perturbing the photovoltaic system and observing the resulting changes in output power. Another approach is the conductance technique, which utilizes the slope of the PV system to determine the point of highest energy. These approaches are further supported by artificial intelligence methods [13][14].

In contrast to traditional two-stage PV systems consisting of a voltage supply electrical converter and a DC-DC boost converter, the Zero Voltage Switching Inverter (ZSI) offers several advantages. It features fewer power switches and can convert the DC voltage from a photovoltaic cell to the desired AC voltage. ZSI provides high-quality power output and incorporates single-stage buck and boost functions. Moreover, ZSI introduces an additional state known as Shoot-through, which is formed by simultaneously operating the upper and lower switches of the same leg. This extra state enables easy control of the voltage with a single-phase configuration [15][16].

The objective of this article is to propose a low-cost solution for current compensation by introducing a three-phase active power filter connected to a PV system through a ZSI [11]. The management of this system is led by the Trigonometric method [17][18], and the DC-side voltage control of the Static Active Power Filter (SAPF) is performed using a standard PI controller [19]. To evaluate the efficiency and performance of the studied system, simulations were conducted using SimPowerSystem in Matlab/Simulink.

The following sections are included in this paper:

Section 2 describes the SAPF topology, which is based on the Z-source inverter. Section 3 discusses the control strategy employed for the SAPF. Simulation results are presented in Section 4. Finally, Section 5 presents the conclusions drawn from this study.

II. SAPF Topology Based on Z-Source Inverter

The configuration of the Z-source SAPF, supported by the PV system, is illustrated in Figure 1. The system consists of a three-phase grid connected to the PV-SAPF system, which caters to both linear and non-linear loads. A 3-leg Z-Source Inverter (ZSI) is connected in parallel with the load through the interfacing inductor. The photovoltaic power generation system comprises a photovoltaic panel, a booster DC-DC converter, and a battery bank. This system supplies DC power to the Z-source grid, ensuring the sustained DC link voltage for the SAPF. The Z-source inverter is utilized to maintain the DC link voltage of the SAPF. In situations where the PV power generation system produces excess power, the surplus energy can be directed through the DC-DC converter circuit to the energy storage unit, enabling the utilization of stored energy from the battery when the PV system output is insufficient [20].

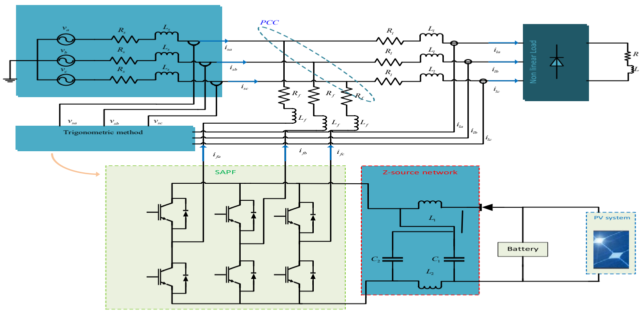

Figure 1 General scheme of SAPF based on two-level ZSI

A. PV Power Generating Unit

The proposed PV power generating unit consists of an SPV (Solar Photovoltaic) panel, a low-step DC-DC boost converter, and a battery. The DC-DC boost converter incorporates an MPPT (Maximum Power Point Tracking) function to optimize power extraction during periods of varying solar irradiation. The output power generated by the PV power generating unit is influenced by factors such as sunlight irradiation and ambient temperature, as described by the relevant equations governing PV cell behavior. Figure 2 illustrates the equivalent circuit of the PV array and DC-DC converter with MPPT control electronics. The PV cell is modeled as a current source connected in parallel with a diode "D". The configuration of the current source and diode is associated with an internal series resistance. The internal resistance of the current source and diode configuration is included in the series circuit. The following equations represent the fundamental characteristics of the PV cell.

$$I_{ph} = I_d + I_{pv} = I_{ph} - I_d \qquad (1)$$

$$V_{pv} = \frac{AkT_c}{e} \ln\left(\frac{I_{ph} + I_d - I_c}{I_d}\right) - R_s I_c \qquad (2)$$

Where I_{pv} represents the PV cell output current in amps and I_d represents the diode reverse saturation current. The voltage across the photovoltaic cell is denoted as:

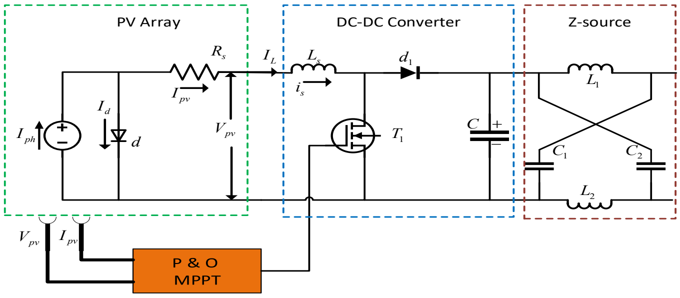

Figure 2 Equivalent circuit of SPV array and DC-DC converter with MPPT control circuitry

The charge strength of the electrons is represented by $\left(1.602\times10^{-19} C\right)$,the output voltage of the photovoltaic cells is denoted as V_{pv} ,and "A" is the curve fitting factor (0.001). The current image is represented by I_{ph} in amps, k is the Boltzmann constant, T_c is the operating temperature of the reference cell $\left(25^{\circ} C\right)$, I_c is the cell's output current in amps, and R_s is the internal resistance of the cell (0.001 Ω).

The output voltage (12V) of the low-pass DC-DC boost converter is supplied to the Z-source inverter to elevate the DC voltage level. This increased DC voltage maintains the DC link of the SAPF. The Z-source inverter operates in two states: shoot through and non-shoot through. During shoot through, both the top and bottom switches of one or more legs of the same phase are turned on simultaneously. The equivalent circuit of the Z-source inverter in the shoot through state is depicted in Figure 3(a). The voltage across the inductor is equal to the voltage across the capacitor (VL = VC) during the shoot-through cycle.

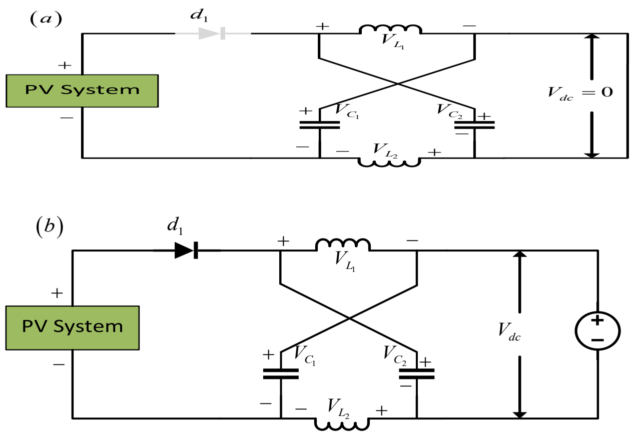

Figure 3 Equivalent circuit of ZSI (a) Shoot through state (b) Non- shoot through state

The equivalent Z-source inverter (ZSI) circuits in the non-shoot through state are illustrated in Figure 3(b), where a three-phase inverter is supplied with the DC voltage. The inverter operates in six switching states. The ZSI modulation pattern is depicted in Figure 4. The total zero-state time remains constant, and each phase leg is switched on and off according to the duty cycle. The shoot through state time is equally distributed among each phase without altering the active state duration. During the non-shoot through state, the voltage across the inductor V_L and the input voltage V_i can be described as follows:

$$V_L = V_{dc} - V_c \qquad (3)$$

The maximum DC-link voltage across the three-phase electrical converter bridge as:

$$V_i = \frac{1}{1-\frac{T_{st}}{T}} V_{dc} \quad (4)$$

$$V_i = BV_{dc} \quad (5)$$

$$B_i = \frac{1}{1-\frac{T_{st}}{T}} \quad (6)$$

Where, $B \geq 1$, B is the boost factor

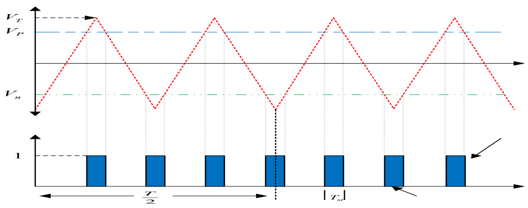

Figure 4 Switching pattern for ZSI

In this context, the shoot-through time per switch cycle remains constant, ensuring a consistent boost factor. To achieve a constant input voltage for the inverter, the shoot-through time per switching cycle is carefully selected. The SAPF with the proposed PV interface operates in three modes: (1) PV power generation mode, (2) Battery backup mode, and (3) Continuous supply mode.

III. Trigonometric method (tri-single-phase method)[21]

The tri-single-phase trigonometric method relies on generating two trigonometric functions, namely sine and cosine, $\cos\,(2.\pi.f.t)$ and $\sin\,(2.\pi.f.t)$ where (f) is the pre-recognized frequency of the power grid voltage, with the pre-determined frequency of the power grid voltage [17][18]. These functions are then used in relation to the load current (I_{L1}, I_{L2}, I_{L3}) to extract its fundamental components. By estimating the active component I_{Lfa} and reactive component I_{Lfr} of each fundamental phase's current, this method enables identification of the current for each phase and facilitates regeneration of the original current. Consequently, a straightforward subtraction is adequate to determine the harmonic current produced by the load.

Consider the load current (I_L) absorbed by the nonlinear load via the first phase:

$$I_L(\theta_s) = \sum_{1}^{\infty} I_L \sin(h\theta_s - \varphi_s) = \sum_{1}^{\infty} I_{L1} \sin(\theta_s - \varphi_1) + \sum_{2}^{\infty} I_L \sin(h\theta_s - \varphi_h) \quad (7)$$

With: $\theta_s = \omega t$

The fundamental component of the voltage at the connection point of the active filter to the first phase, is expressed by:

$$v_{sa}(\theta_s) = v_s\sqrt{2}\sin(\theta_s) \quad (8)$$

By multiplying the equation (7) by $\sin(\theta_s)$ *and* $\cos(\theta_s)$ we get the expressions (9) and (10) respectively:

$$I_{L1}(\theta_s)\sin(\theta_s) = \frac{I_{L1}}{2}\cos(\varphi_1) - \frac{I_{L1}}{2}\cos(2\theta_s - \varphi_1) + \sin(\theta_s)\sum_{h=2}^{\infty} I_L \sin(h\theta_s - \varphi_h) \quad (9)$$

$$I_{L1}(\theta_s)\cos(\theta_s) = \frac{I_{L1}}{2}\sin(\varphi_1) + \frac{I_{L1}}{2}\cos(2\theta_s - \varphi_1) + \cos(\theta_s)\sum_{h=2}^{\infty} I_L \sin(h\theta_s - \varphi_h) \quad (10)$$

The equations (9) and (10) demonstrate that only the steady components are directly proportional to the amplitude of the active fundamental current and the amplitude of the reactive current, respectively. Additionally, the first harmonic components have a frequency twice that of the power network. Hence, these AC components need to be filtered out using a low-pass filter with a relatively low cutoff frequency to prevent the propagation of low-frequency ripple at the output. However, striking the right balance between effective filtering of parasitic frequencies and maintaining a fast extraction algorithm dynamics can be challenging.

After filtering, we get:

$$\left[I_{L1}(\theta_s)\sin(\theta_s)\right]_{filtre} = \frac{I_{L1}}{2}\cos(\varphi_1) \quad (11)$$

$$\left[I_{L1}(\theta_s)\cos(\theta_s)\right]_{filtre} = \frac{I_{L1}}{2}\sin(\varphi_1) \quad (12)$$

We can then reconstitute the fundamental current. Thus, by multiplying (11) and (12) respectively by $2\sin(\theta_s)$ *and* $2\cos(\theta_s)$, we deduce the following fundamental current equation:

$$I_{Lf} = I_{L1}(\theta_s)\sin(\theta_s) - I_{L1}\sin(\varphi_1) - \cos(\theta_s) = I_{Lfa} + I_{Lfr} = I_{L1}\sin(\theta_s - \varphi_1) \quad (13)$$

A. Identification algorithm

The figure below illustrates the algorithm for extracting the fundamental current according to the tri-phase method.

$$I_{L1} = I_L - I_{L1f}$$

I_L : Current of the disturbed load;

I_{L1f} : fundamental component of the disturbed current;

I_{L1} : harmonic component of the disturbed current.

This extraction method can be applied to both single-phase and three-phase systems without the need for mains voltage.

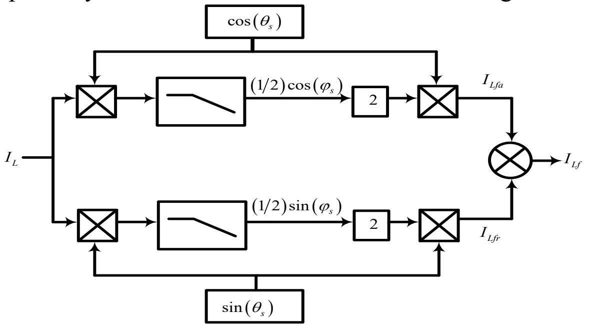

Figure 5 Fundamental extraction algorithm by the tri-single-phase method

B. Hysteresis control

The hysteresis current control principle aims to maintain each of the generated currents within a specific range around the reference currents. If any deviation from this range occurs, a commutation command is triggered to bring the currents back within the desired band.

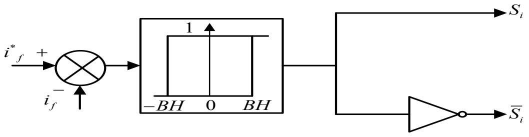

Figure 6 Hysteresis band current controller

C. Fixed band hysteresis control

In this type of current control, the switching frequency primarily relies on the rate of change of the desired current. This rate of change is influenced by the decoupling inductance's magnitude and the voltage drop across it. The filtering mechanism impacts both the switching frequency and the dynamic response of the active filter. The key advantage of this method is its simple implementation. However, its main drawback is the variable switching frequency, which may lack proper control [22].

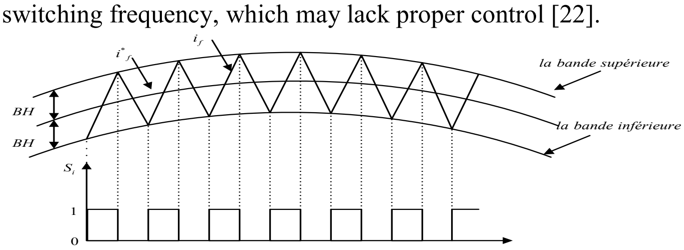

Figure 7 Control of switches by fixed band hysteresis

IV. Simulation Results

The parameters of the PV-SAPF system are presented in Table 1. Simulation studies were conducted using MATLAB/Simulink to evaluate the performance of the PV-SAPF system. The results before and after connecting the PV-SAPF system are presented. It should be noted that the initial voltage state of the capacitors in the system is zero

Table 1. Parameters of system

Parameters		Value
System voltages (line to line) Vrm		$57V$
Frequency	f	$50Hz$
Filter (series SAPF)	L_s, R_s	$0.45\Omega, 2.5mH$
Battery voltage		$30V$
Battery capacity		$33Ah$
Filter (shunt SAPF)	L_f, R_f	$0.9\Omega, 4mH$
DC-DC converter		
Inductor	$L_{z-source}$	$5mH$
Capacitance	$C_{z-source}$	$1100\mu F$
Switching frequency	$f_{z-source}$	$1KH$
Proportional gain	K_p	6.8
Integral gain	K_i	1.1
Sample time		$1e^{-4}$
Charge non-linéaire	R_C	17Ω

A. DC Voltage Variation

First, the performance of a conventional PI controller and its response to a step change in the DC bus voltage from 160 to 140 V is confirmed in Figure 8. Clearly, the conventional PI controller yields highly satisfactory outcomes.

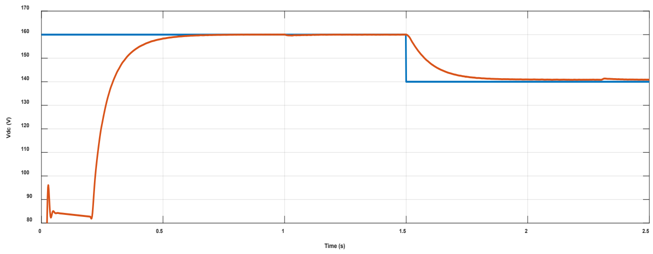

Figure 8 illustrates the simulation results depicting the response of the DC bus voltage to a conventional PI-based reference DC voltage variation.

B. Continuous operation

The results of the system state before and after the connection of the filter are presented in Figures 9 to 11. The performance of the PV compliant ZSI-SAPF is evaluated under balanced voltage and load currents. Figure 9 displays the source current prior to connecting the ZSI-based SAPF. Figure 10 showcases the source current, filter current, and DC bus voltage after the filter connection. It is evident that the source current exhibits a pure sinusoidal waveform following the filter connection.

The current source was analyzed using the Fast Fourier Transform (FFT) analysis tool, and the simulation results are depicted in Figure 11. The waveform before filtering exhibits significant distortion, as evidenced by the spectral analysis graph, which displays the presence of odd harmonics in the signal except for multiples of the third harmonic. However, after filtering, the current waveform becomes sinusoidal, effectively suppressing the harmonic components. Only the fundamental component is visible in the spectral display, indicating successful harmonic suppression.

Consequently, the measured Total Harmonic Distortion of current (THDi) is successfully reduced to 0.72% after compensation in the simulation. These results are in compliance with the requirements of the international standard IEEE-519 [23].

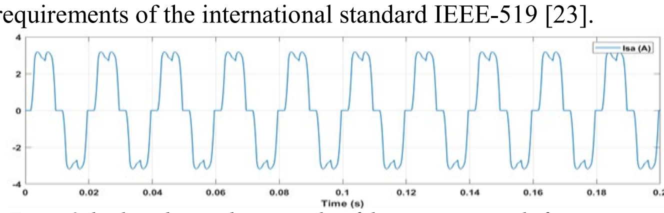

Figure 9 displays the simulation results of the source current before connecting the filter

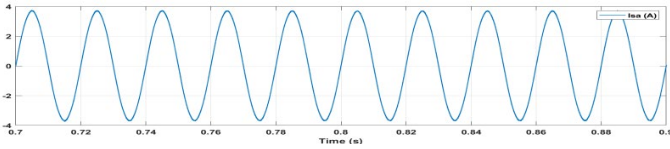

(a)

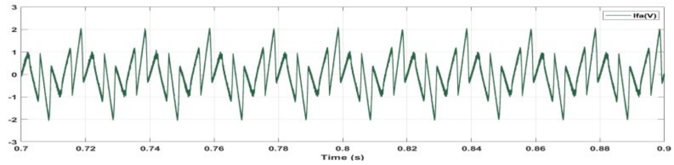

(b)

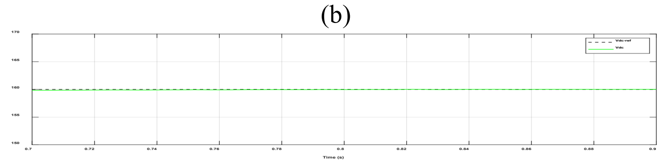

(c)

Figure 10 Simulation results of (a) source current , (b) filter current , and (c) DC bus voltage , after the implementation of ZSI-SAPF.

(a)

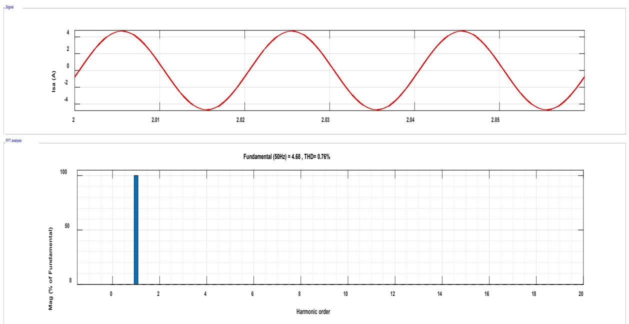

(b)

Figure 11 Simulation results of the harmonics spectrum of source current before (a) and after (b) the implementation of ZSI-SAPF.

Figure 13 illustrates the results of the source current, filter current, and DC bus voltage when the filter is connected. Prior to connecting the filter, the load current is solely provided by the network. The capacitors in the Z-source network are charged from the battery bank, which in turn is charged by the Solar Photovoltaic (SPV) system, until the capacitors reach the line voltage level.
Upon connection, the SPV compliant ZSI-SAPF begins injecting the necessary electric current to eliminate harmonics from the source current. The PI controller maintains the voltage level at the desired reference value. Notably, after connecting the filter, the presence of ripple in the active and reactive powers is eliminated, leading to successful compensation of reactive power.

The proposed SPV-compliant ZSI-SAPF system with a PI controller demonstrates comparable reliability, simplicity, and effectiveness in enhancing power quality when compared to recently published SAPF systems. The results of the comparison, presented in Table 2, highlight the superiority of the proposed system over other methods.

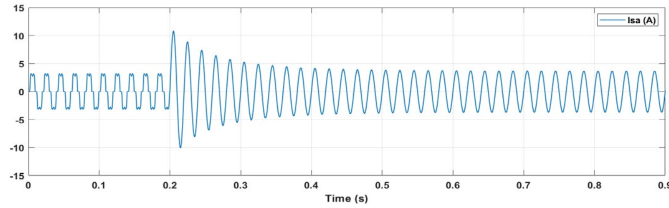

(a)

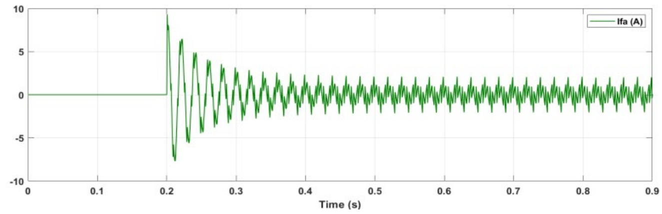

(b)

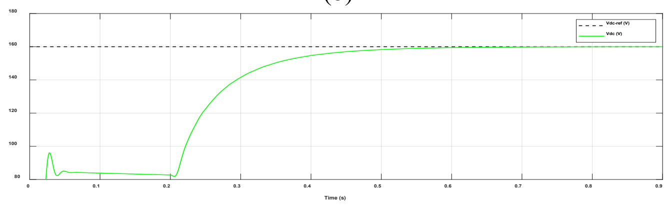

(c)

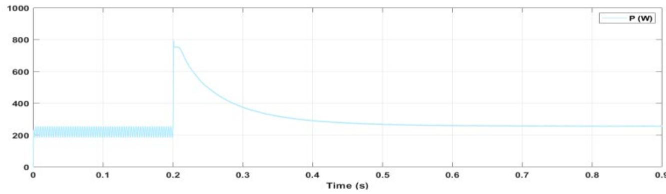

(d)

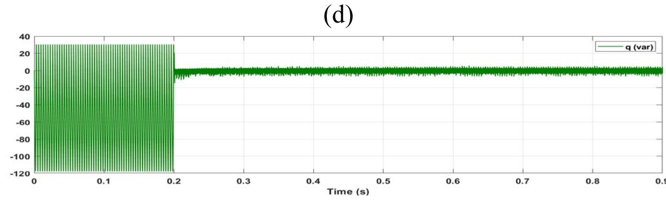

(e)

Fig. 13 Waveforms of the system parameters under ZSI-SAPF switched

Table 2. Comparison results between the proposed and different control strategies

Topology	**Control strategy**	**Simulation results of THD source current**	
		before connecting SAPF	**after connecting SAPF**
SAPF	(p–q) method proposed in [3]	20.03%	1.78%
SAPF	DPC strategy proposed in [3]	/	1.16%
SAPF	Predictive-DPC-SVM strategy proposed in [3]	/	0.90%
SAPF	Predictive control strategy proposed i [24]	22.60%	0.81%
ZSI-SAPF	trigonometric method	23.18%	0.76%

V. Conclusion

This paper proposes a design for a three-phase shunt active power filter based on a Z-source inverter controlled by a trigonometric method and a PI hysteresis control algorithm. The proposed structure aims to compensate for harmonic components caused by nonlinear loads. The performance of the proposed structure was evaluated under various operating conditions using a non-linear load, and simulation results in MATLAB/Simulink demonstrate satisfactory performance.

Furthermore, the proposed structure exhibits improved efficiency compared to the conventional structure, highlighting its effectiveness. The simulation test also demonstrates that the proposed structure achieves the best Total Harmonic Distortion of current (THDi) at 0.76%. To further enhance system performance, the control algorithm can be extended to optimize the parameters of the PI controller.

Moreover, the proposed structure ensures unit power factor operation since the reactive power is nearly zero, emphasizing its ability to maintain power factor close to unity. Several inferences can be summarized from this work:

The proposed shunt active power filter based on a Z-Source inverter successfully restored the distorted current source to its original sinusoidal waveform.

The investigations conducted demonstrated that the proposed filter effectively minimized current harmonics well below the limits specified by the IEEE standard.

The FFT spectrum analyses revealed that the implementation of the proposed ZSI-SAPF resulted in a significant reduction in Total Harmonic Distortion (THD), reducing it from 23% to 0.76%.

The evaluation of the proposed shunt active power filter based on the Z-Source inverter showcased its effectiveness in mitigating harmonic currents under various operating conditions. Furthermore, a comparative study highlighted that the performance of this system surpassed other existing approaches in the literature when evaluated under similar operating conditions.

To further enhance the system, it is suggested to establish and verify the proposed approach through the development of a prototype model. Additionally, extending the control algorithm to optimize the parameters of the PI controller can be considered.

REFERENCES

[1] B. Mansour, B. Abdelkader, and B. Said, “Application of backstepping to the virtual flux direct power control of five-level three-phase shunt active power filter,” *Int. J. Power Electron. Drive Syst.*, vol. 4, no. 2, p. 173, 2014.

[2] H. Akagi, “Modern active filters and traditional passive filters,” *Bull. Polish Acad. Sci. Tech. Sci.*, pp. 255–269, 2006.

[3] A. Krama, L. Zellouma, A. Benaissa, B. Rabhi, M. Bouzidi, and M. F. Benkhoris, “Design and Experimental Investigation of Predictive Direct Power Control of Three-Phase Shunt Active Filter with Space Vector Modulation using Anti-windup PI Controller Optimized by PSO,” *Arab. J. Sci. Eng.*, vol. 44, no. 8, pp. 6741–6755, 2019, doi: 10.1007/s13369-018-3611-6.

[4] V. Mahajan, P. Agarwal, and H. O. Gupta, “Implementation of high-voltage multilevel harmonic filter based on rotated carrier modulation and artificial intelligence-based controllers,” *Arab. J. Sci. Eng.*, vol. 39, pp. 7127–7143, 2014.

[5] F.-Z. Peng, H. Akagi, and A. Nabae, “A study of active power filters using quad-series voltage-source PWM converters for harmonic compensation,” *IEEE Trans. Power Electron.*, vol. 5, no. 1, pp. 9–15, 1990.

[6] H. Sasaki and T. Machida, “A new method to eliminate AC harmonic currents by magnetic flux compensation-considerations on basic design,” *IEEE Trans. Power Appar. Syst.*, no. 5, pp. 2009–2019, 1971.

[7] L. Zellouma, S. Saad, N. Debbache, and A. Omeiri, “Etude de l’auto-adaptivité du filtre actif parallèle aux variations de la charge,” *Synthèse Rev. des Sci. la Technol.*, vol. 17, pp. 64–72, 2008.

[8] A. Chebabhi, M. K. Fellah, A. Kessal, and M. F. Benkhoris, “Comparative study of reference currents and DC bus voltage control for Three-Phase Four-Wire Four-Leg SAPF to compensate harmonics and reactive power with 3D SVM,” *ISA Trans.*, vol. 57, pp. 360–372, 2015.

[9] S. Saidi, R. Abbassi, and S. Chebbi, “Quality improvement of shunt active power filter with direct instantaneous power estimator based on Virtual Flux,” *Int. J. Control. Autom. Syst.*, vol. 14, pp. 1309–1321, 2016.

[10] V. K. A. Shankar and N. S. Kumar, “Implementation of shunt active filter for harmonic compensation in a 3 phase 3 wire distribution network,” *Energy Procedia*, vol. 117, pp. 172–179, 2017.

[11] S. Parthiban and V. Madhaiyan, “Experimental validation of solar PV sustained ZSI based unified active power filter for enrichment of power quality,” *Automatika*, vol. 62, no. 1, pp. 137–153, 2021.

[12] V. Madhaiyan and V. Subramaniam, “Extended reference signal generation scheme for integration of unified power quality conditioner in grid-connected photovoltaic system,” *Electr. Power Components Syst.*, vol. 43, no. 8–10, pp. 914–927, 2015.

[13] M. A. Mansor, K. Hasan, M. M. Othman, S. Z. B. M. Noor, and I. Musirin, “Construction and performance investigation of three-phase solar PV and battery energy storage system integrated UPQC,” *Ieee Access*, vol. 8, pp. 103511–103538, 2020.

[14] J.-M. Kwon, K.-H. Nam, and B.-H. Kwon, “Photovoltaic power conditioning system with line connection,” *IEEE Trans. Ind. Electron.*, vol. 53, no. 4, pp. 1048–1054, 2006.

[15] J. Abbasi Bolaghi, A. Taheri, and M. H. Babaei, “Switched-capacitor inductor Z-source inverter with an impedance network,” *Int. Trans. Electr. Energy Syst.*, vol. 31, no. 5, p. e12529, 2021.

[16] F. Z. Peng, M. Shen, and Z. Qian, “Maximum boost control of the Z-source inverter,” *IEEE Trans. power Electron.*, vol. 20, no. 4, pp. 833–838, 2005.

[17] D. O. Abdeslam, P. Wira, J. Mercklé, Y.-A. Chapuis, and D. Flieller, “Stratégie neuromimétique d’identification et de commande d’un filtre actif parallèle,” *Rev. Int. du Génie Electrique,(RS-RIGE) p*, pp. 35–64, 2006.

[18] A. L. de Heredia Bermeo, “Commandes avancées des systèmes dédiés à l’amélioration de la qualité de l’énergie: de la basse tension à la montée en tension.” Institut National Polytechnique de Grenoble-INPG, 2006.

[19] J. H. Van der Lee, W. Y. Svrcek, and B. R. Young, “A tuning algorithm for model predictive controllers based on genetic algorithms and fuzzy decision making,” *ISA Trans.*, vol. 47, no. 1, pp. 53–59, 2008.

[20] A. Abdelkarim, B. Youcef, L. Zellouma, D. Toumi, A. Ibrahim, and R. Aboelsaud, “Improved space vector modulation algorithm of 5-level three-phase z-source based cascaded inverter,” *Int. J. Power Electron. Drive Syst.*, vol. 13, no. 4, p. 2286, 2022.

[21] O. MOUSSA, “Etude des harmoniques et techniques de commandes du filtre actif.” Université de Batna 2, 2016.

[22] A. Tripathi and P. C. Sen, “Comparative analysis of fixed and sinusoidal band hysteresis current controllers for voltage source inverters,” *IEEE Trans. Ind. Electron.*, vol. 39, no. 1, pp. 63–73, 1992.

[23] R. Langella, A. Testa, and E. Alii, “IEEE recommended practice and requirements for harmonic control in electric power systems,” in *IEEE Recommended Practice*, IEEE, 2014.